

# Numerically exact computation of the optical properties of light absorbing carbon aggregates for wavelength of 200 nm–12.2 $\mu\text{m}$

M. Kahnert

Swedish Meteorological and Hydrological Institute, 601 76 Norrköping, Sweden

Received: 16 March 2010 – Published in Atmos. Chem. Phys. Discuss.: 6 May 2010

Revised: 31 August 2010 – Accepted: 1 September 2010 – Published: 6 September 2010

**Abstract.** The optical properties of externally mixed light absorbing carbon (LAC) aggregates are computed over the spectral range from 200 nm–12.2  $\mu\text{m}$  by use of the numerically exact superposition T-matrix method. The spectral computations are tailored to the 14-band radiation model employed in the Integrated Forecasting System operated at the European Centre for Medium Range Weather Forecast. The size- and wavelength dependence of the optical properties obtained with the fractal aggregate model differs significantly from corresponding results based on the homogeneous sphere approximation, which is still commonly employed in climate models. The computational results are integrated into the chemical transport model MATCH (Multiple-scale Atmospheric Transport and CHEmistry modelling system) to compute 3-D fields of size-averaged aerosol optical properties. Computational results obtained with MATCH are coupled to a radiative transfer model to compute the shortwave radiative impact of LAC. It is found that the fractal aggregate model gives a shortwave forcing estimate that is twice as high as that obtained with the homogeneous sphere approximation. Thus previous estimates based on the homogeneous sphere model may have substantially underestimated the shortwave radiative impact of freshly emitted LAC.

## 1 Introduction

Light absorbing carbon (LAC, also called black carbon) in the atmosphere originating from soot and biomass burning emissions has been identified as the second most important primary cause for global warming after  $\text{CO}_2$  (Ramanathan and Carmichael, 2008). LAC global forcing estimates range between 0.4 to 1.2  $\text{W/m}^2$ , which is as much as 55 % of the

forcing of  $\text{CO}_2$ , and more than the forcing caused by all other greenhouse gases combined (Forster et al., 2007). LAC aerosols increase the energy in the atmosphere, reduce the radiative flux at the surface, and increase the radiative forcing at the top of the atmosphere. LAC is a short-lived warming agent, so emission reductions would have an immediate effect to slow down global warming. Therefore the radiative impact of this aerosol species is of considerable interest for both researchers and policy makers.

Uncertainties in the direct radiative forcing estimate of aerosols are commonly believed to be mainly caused by uncertainties in the aerosol fields employed in climate models. Thus the trend in modern climate models is to replace climatological by dynamic descriptions of aerosol fields by coupling atmosphere-ocean general circulation models (GCMs) to chemical transport models (CTMs). Dynamically coupled atmosphere-ocean-chemistry-vegetation models are often referred to as Earth system models. To constrain the direct radiative forcing estimates of LAC in Earth system models, efforts are focusing on revising emission estimates of soot and biomass burning aerosols, understanding the internal mixing of LAC with other aerosol species, and improving the description of vertical mixing and removal processes. Little attention is paid in climate modelling to the effect of particle morphology on the radiative impact of aerosols. It is often taken for granted that the use of Lorenz-Mie theory and the assumption that aerosols are homogeneous particles with perfect spherical symmetry gives a sufficiently accurate description of the aerosol optical properties (AOPs) of LAC for the purpose of radiative flux computations. However, evidence has been found that the mixing state of chemically heterogeneous aerosols can be important for the radiative impact of aerosols (Jacobson, 2001). Also, it has been demonstrated for mineral aerosols that nonspherical particles give a significantly different radiative impact than homogeneous spherical model particles (e.g. Pilinis and Li, 1998; Kahnert et al., 2007; Otto et al., 2009).



Correspondence to: M. Kahnert  
(michael.kahnert@smhi.se)

It has long been recognised by combustion researchers, electrical engineers, astrophysicists, and aerosol scientists that the spectral optical properties of aggregated particles and the dependence of AOPs on size, refractive index, and scattering angle can strongly deviate from those of size-equivalent homogeneous spheres (e.g. Mackowski, 1994; Sorensen, 2001; Bond and Bergstrom, 2006; Liu et al., 2008; Okada et al., 2008; Zhao and Ma, 2009). However, in climate applications, one is only interested in broadband net fluxes, i.e. radiance computations integrated over directional angles and wavelengths. Broadband net fluxes are believed to be less sensitive to aerosol morphology than spectral and differential AOPs. Also, computing the AOPs of realistic fractal LAC aggregates is a highly complex problem, and it did not seem computationally feasible to apply realistic models in conjunction with numerically exact electromagnetic scattering computations to broadband applications. On the other hand, approximate electromagnetic solution methods, such as the Rayleigh-Debye-Gans approximation, did not give the desired accuracy (Bond and Bergstrom, 2006).

In a recent study (Kahnert, 2010a), numerically exact computations of the optical properties of LAC aggregates at wavelengths of 440 nm and 870 nm were coupled to a regional CTM and to radiative transfer computations. The numerical computations proved to be efficient and robust, and it seems highly probable that the same numerical method can be applied to broadband computations. It was found that at 440 nm the spectral radiative impact computed with aggregates and homogeneous spheres were significantly different. By contrast, at 870 nm the radiative net fluxes were comparable on account of some lucky error cancellations between the effects of scattering and absorption. Thus it is not clear a priori how large an error one introduces in broadband radiative net flux computations if one does not account for the complex morphological properties of LAC aggregates. The aim of the present study is to compute AOPs of LAC by use of a rigorous solution to Maxwell's equations for fractal aggregates, to perform numerical computations over the entire shortwave range relevant for climate applications, to integrate the results into a CTM, and to apply the results in a broadband radiative transfer test case. Section 2 introduces the methodology, Sect. 3 presents results, and Sect. 4 offers conclusions.

Note that this study focuses on externally mixed LAC aggregates. External mixing is characteristic for freshly emitted LAC. As LAC ages in the atmosphere, it gets oxidised and becomes partially hydrophilic, while its fractal dimension increases. Aged LAC aggregates are usually internally mixed with other water-soluble aerosol components. The optical properties of internally mixed LAC are discussed by several authors (Fuller, 1995; Videen and Chýlek, 1998; Fuller et al., 1999; Jacobson, 2000; Mishchenko et al., 2004; Bond et al., 2006; Kocifaj and Videen, 2008; Worringer et al., 2008).

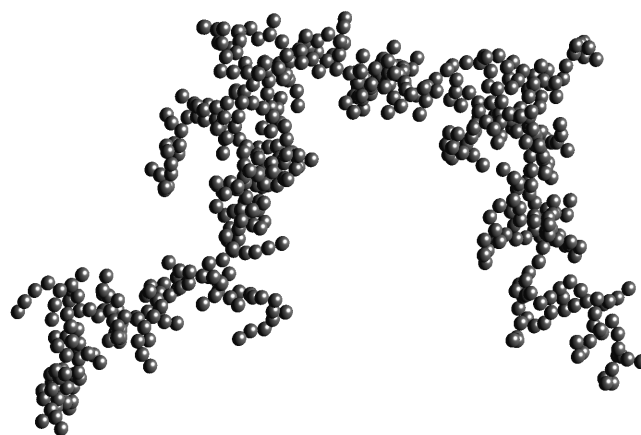


**Fig. 1.** Light absorbing carbon aggregate with  $N_s=600$  primary monomers, fractal dimension  $D_f=1.82$ , and structure factor  $k_0=1.27$ .

## 2 Methods

### 2.1 Modelling optical properties of LAC aggregates

The broadband computations performed in this study are geared to the new 14-band shortwave radiation scheme of the Integrated Forecasting System (IFS) developed and operated at the European Centre for Medium Range Weather Forecast (ECMWF). The shortwave bands cover a range of wavelengths from 200 nm to 12.2  $\mu\text{m}$ . We compute AOPs of LAC as a function of particle size for a total of 16 wavelengths, namely, for each of the 14 band mid-points, as well as for the minimum and maximum wavelengths  $\lambda=200$  nm and  $\lambda=12.2$   $\mu\text{m}$ . A description of the IFS radiation scheme can be found in the online documentation of IFS (<http://www.ecmwf.int/research/ifsdocs/CY33r1/PHYSICS/IFSPart4.pdf>).

The AOPs are computed by representing the externally mixed LAC aerosols as fractal aggregates, such as that shown in Fig. 1. Our objective is to perform computations that cover the entire space of relevant sizes and wavelengths. Since numerical AOP computations of aggregated particles are challenging and time consuming, this leaves very little room for performing, e.g., ensemble averages over a large number of particle geometries. We therefore need to identify a selection of representative model geometries. It is rather fortunate and truly remarkable that this is indeed possible to achieve by classifying aggregate geometries according to the scaling relation

$$N_s = k_0 \left( \frac{R_g}{a} \right)^{D_f}. \quad (1)$$

Here the aggregate is composed of  $N_s$  spherical monomers of equal radius  $a$ ,  $D_f$  and  $k_0$  are known as the fractal dimension and fractal prefactor, and  $R_g$  denotes the radius of gyration of the aggregate. The latter is defined by

$$R_g = \sqrt{\frac{1}{N_s} \sum_{i=1}^{N_s} r_i^2}, \quad (2)$$

where  $r_i$  denotes the distance of the  $i$ th monomer from the aggregate's centre of mass.

The scaling relation given in Eq. (1) defines a class of aggregate geometries. All members of such a class have very similar optical properties. Thus, the problem of identifying representative model geometries is reduced to identifying the parameters that occur in the scaling relation (1). The ranges of most of these parameters can be narrowed down significantly (Bond and Bergstrom, 2006). We assume that the aggregates have a fractal dimension  $D_f=1.82$  and a fractal prefactor  $k_0=1.27$ . These values are supported by both diffusion limited cluster aggregation simulations and by measurements (Sorensen and Roberts (1997); see also Bond and Bergstrom (2006) and references therein). The refractive index is the most critical input parameter to the AOP computations. In a recent study Bond and Bergstrom (2006) were able to demonstrate that the refractive index of LAC varies over a much smaller range than previously assumed. For the spectral variation of the refractive index of LAC we rely on the measurements by Chang and Charalampopoulos (1990). These measurements are consistent with the void-fraction model discussed by Bond and Bergstrom (2006). The primary monomers are assumed to have a radius of  $a=25$  nm, which gives the most reasonable results for the single-scattering albedo (Kahnert, 2010b). The absorption cross section is completely insensitive to a variation in  $a$  for  $a \leq 40$  nm (Bond and Bergstrom, 2006).

We generate our model geometries by use of a random cluster generation algorithm, which was developed by Mackowski (1994). As mentioned above, the essential idea of the scaling relation given in Eq. (1) is to define a class of geometries that have well constrained optical properties. The total absorption and scattering cross sections display indeed very little variation among different geometries that obey the same scaling relation. However, computational results reported by Kahnert (2010a,b) indicate that differential scattering properties, such as the backscattering cross section  $C_{\text{bak}}$ , may not be sufficiently well constrained by specifying  $\{a, N_s, D_f, k_0\}$ . This can give rise to numerical artifacts in the form of fluctuations of  $C_{\text{bak}}$  as a function of aggregate size. Although  $C_{\text{bak}}$  does not enter into the computation of the radiative impact of aerosols, we shall test a pragmatic and computationally inexpensive approach for alleviating the fluctuation problem associated with  $C_{\text{bak}}$ . In principle one could repeat computations for an ensemble of different geometries and compute ensemble-averaged AOPs. However, for the broadband calculations we intent to perform, such an approach would be

prohibitively time consuming. We therefore try to identify, for each size, a “typical” geometry that gives a value of  $C_{\text{bak}}$  close to the mean. To this end, we select a single wavelength of  $\lambda=533.2$  nm, and compute the AOPs as a function of size for five different geometries at each discrete size. Although a sample of only five geometries is not expected to give a highly accurate estimate of the mean value of  $C_{\text{bak}}$ , this approach proves to be sufficiently robust for reducing the fluctuations of  $C_{\text{bak}}$  as a function of size, while keeping the computational costs within reasonable limits. Figure 2 shows computational results represented by circles for the absorption cross section  $C_{\text{abs}}$  (upper left), the scattering cross section  $C_{\text{sca}}$  (upper right), the asymmetry parameter scaled by the scattering cross section  $g \times C_{\text{sca}}$  (lower left), and the backscattering cross section  $C_{\text{bak}}$  (lower right). The AOPs are presented as functions of the volume-equivalent radius  $R_V$ . The quantities that are important for radiative transfer computations are  $C_{\text{abs}}$ ,  $C_{\text{sca}}$ , and  $g \times C_{\text{sca}}$ . The five different geometries yield almost identical results for these optical properties. By contrast,  $C_{\text{bak}}$  displays some variation (note the logarithmic scale!). We compute at each particle size  $R_V$  an average  $\langle C_{\text{bak}} \rangle$ . Next we select for each particle size  $R_V$  that geometry that yields a value of  $C_{\text{bak}}$  closest to  $\langle C_{\text{bak}} \rangle$ . The computed AOPs obtained for these “typical” geometries are indicated by the green pluses in Fig. 2. Comparison with the red fitting curves shows that these geometries indeed yield a smooth size dependence for all AOPs, thus significantly reducing the fluctuations of  $C_{\text{bak}}$  as a function of  $R_V$ . These “typical” geometries are the ones we employ for the broadband calculations. So in the broadband computations, we only employ one geometry for each size  $R_V$ . This approach reduces numerical artifacts sufficiently well without increasing the required computation time.

The AOPs of the aggregates are computed by use of the numerically exact superposition T-matrix method for solving Maxwell's equations for fractal aggregates, which has been developed by Mackowski and Mishchenko (1996). The computer code for performing numerical orientation averaging has been developed by Okada and Kokhanovsky (2009). Computations are performed for eight discrete aggregate sizes between  $N_s=7$  and  $N_s=600$ , where the intermediate points are chosen such that the corresponding volume-equivalent radii  $R_V$  are equally spaced. For a monomer radius of  $a=25$  nm, this range of  $N_s$  very well covers the range of typical mass-per-particle values (Kahnert, 2010a). Note, however, that LAC aggregates in nature can be composed of monomers with radii as small as  $a=10$  nm, in which case  $N_s$  can be larger than 1000. However, as discussed by Kahnert (2010b), the model aggregates with  $a=25$  nm seem to yield the best agreement with measured optical properties, as discussed in the following section.

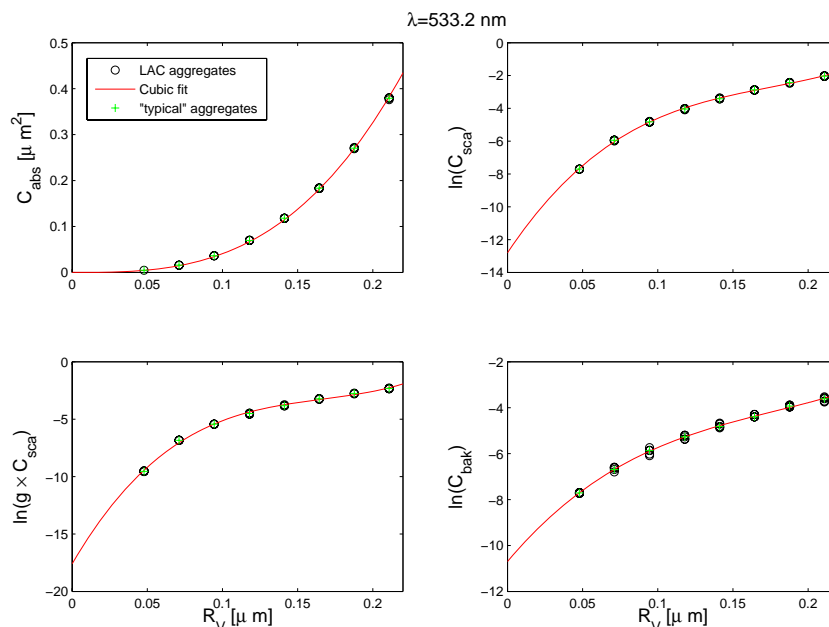


**Fig. 2.**  $C_{\text{abs}}$  (upper left),  $C_{\text{sca}}$  (upper right),  $g \times C_{\text{sca}}$  (lower left), and  $C_{\text{bak}}$  (lower right) computed for five different model geometries (circles) at  $\lambda=533.2$  nm. The green pluses denote results obtained for “typical” model geometries as explained in the text. The fitting curves are explained in the next section.

## 2.2 Comparison with measurements, sensitivity tests, and comparison of approximate and exact computational methods

Before we can perform broadband AOP computations suitable for climate modelling, we need to discuss three essential issues. The most important issue is the comparison of AOP modelling results with measurements. The second issue is the sensitivity of the AOP modelling results to variations in particle morphology and refractive index. The third issue is the numerical method employed for solving the electromagnetic scattering problem (i.e. approximate methods or methods based on rigorous electromagnetic theory). A recent study (Kahnert, 2010b) was dedicated to investigating these topics. In this section we briefly review the main results of this investigation.

Bond and Bergstrom (2006) reviewed 21 publications of measured mass absorption cross sections (MAC) and six publications reporting measurements of the single scattering albedo  $\omega$  of LAC. Based on this review they concluded that at a wavelength of 550 nm the most reasonable estimates for these parameters are  $\text{MAC}=(7.5\pm 1.2) \text{ m}^2/\text{g}$  and  $\omega=(0.25\pm 0.05)$ . As shown by Kahnert (2010b), computational results obtained with the aggregate model agree with measured MAC within the range of uncertainty if assuming an LAC mass density of  $\rho=1.5 \text{ g}/\text{m}^3$ . The computational results for MAC are most sensitive to the choice of refractive index. Within the range of fractal dimensions typically observed for atmospheric LAC, the AOPs are much less sensi-

tive to a variation in the fractal parameters than to a variation in the refractive index (Kahnert, 2010b; see also Liu et al., 2008). Computational results for MAC were found to be completely insensitive to a variation in the monomer radius  $a$  (Kahnert, 2010b). The latter had been restricted to  $a=10\text{--}25$  nm, which is the range typically observed for atmospheric LAC aggregates (Bond and Bergstrom, 2006). On the other hand, it was found (Kahnert, 2010b) that the single scattering albedo  $\omega$  is rather sensitive to a variation in  $a$ . The best agreement between modelled and measured values of  $\omega$  is obtained for  $a=25$  nm, which is the value of  $a$  we use in the present study.

Numerical solution methods of the electromagnetic scattering problem have been developed that can partially or completely neglect interaction among monomers in the aggregate (e.g. Xu and Gustafson (2001)). Such approximations can greatly expedite numerical calculations. However, it has been shown by Kahnert (2010b) that such ad hoc approximations can introduce substantial errors in calculations of the optical properties of LAC. For this reason, the present study employs a numerically exact superposition T-matrix code (Mackowski and Mishchenko, 1996). The term “numerically exact” is commonly used to characterise methods for which the computational accuracy is only limited by approximations in the numerical implementation, such as discretisations or truncation of infinite series, rather than by neglecting physical processes in the formulation of the method.

### 2.3 Chemical transport and radiative transfer modelling

The results of the aerosol optics computations are integrated into the Multiple-scale Atmospheric Transport and Chemistry modelling system (MATCH) (Andersson et al., 2007). This CTM computes, apart from reactive gases, 3-D fields of size-resolved chemical composition of aerosols. In this study, we employ a simple model version with 4 size classes for internally mixed and 4 size classes for externally mixed aerosol species. LAC is assumed to only occur in the Aitken and Accumulation size classes. Sulphate, nitrate, ammonium, sea salt, and water-soluble organic carbon (OC) are assumed to be internally mixed. Their refractive indices are computed on-line by use of effective medium theory (Maxwell-Garnett, 1904; Bruggemann, 1935). Mineral dust and non-soluble OC are treated as externally mixed aerosols. The AOPs of all aerosol components other than LAC are computed off-line by use of the homogeneous sphere approximation (HSA). The AOPs are integrated off-line over the aerosol size classes employed in the MATCH model. The size-integrated AOPs are read in by MATCH and coupled to the aerosol size distributions computed by MATCH for each grid cell of the 3-D model domain. Thus the model computes 2-D fields of aerosol optical depth (AOD), and 3-D fields of extinction coefficient, backscattering coefficient, single scattering albedo  $\omega$ , asymmetry parameter  $g$ , and transmission length/visibility. Since the AOP look-up table is computed off-line, the CPU time requirements for computing size- and composition-averaged AOP within MATCH is negligible compared to the computational efforts involved in computing chemical transformation, transport, and deposition.

Note that many studies have demonstrated the inadequacy of the HSA for nonspherical mineral dust particles (e.g. Kahnert and Nousiainen (2006); Veihelmann et al. (2006); Kahnert (2004); Schulz et al. (1999a, 1998)). The HSA may even be one of the dominant sources of error in quantifying the radiative forcing effect of mineral dust (Kahnert and Kylling, 2004; Kahnert et al., 2005, 2007; Otto et al., 2009). For the present study we focus entirely on externally mixed LAC and neglect the significance of aerosol morphology for the AOPs of mineral dust. Note further that we neglect here the important effect of internal mixing of LAC, which can significantly enhance the radiative forcing effect of LAC (Bond et al., 2006).

The MATCH model is currently not yet coupled online to a numerical weather prediction or climate model. Thus the model does not have a fast 3-D radiative transfer code. To obtain a first estimate of the error in broadband radiative impact calculations of LAC introduced by the HSA, we select a vertical profile of AOPs computed with MATCH and use these results as input to the 1-D radiative transfer model DISORT (Stamnes et al., 1988). Calculations are performed with LAC AOPs computed both with the aggregate model and with the HSA, and the radiative impacts are compared.

The DISORT model solves the radiative transfer equation by Fourier-transforming with respect to the azimuthal coordinate, and by discretising the equations for each Fourier mode with respect to the polar and vertical coordinates. In this way, the integro-differential radiative transfer equation is reformulated as an eigenvalue problem for each Fourier mode. The only physical approximation in DISORT is that polarisation effects are neglected. Note, however, that there also exists the polarised version VDISORT that computes all four components of the Stokes vector (Weng, 1992; Schulz et al., 1999b; Schulz and Stamnes, 2000).

Vertical profiles of optical properties computed with MATCH are used as input to DISORT to compute for each wavelength band  $l$  a  $\lambda$ -integrated radiative net flux  $F_l^{\text{net}} = F_l^{\text{s}} + F_l^- - F_l^+$ . Here  $F_l^{\text{s}}$  is the direct solar flux integrated over band  $l$ , i.e. that part of the incoming flux that survives extinction,  $F_l^-$  represents the diffuse downwelling flux, and  $F_l^+$  denotes the upwelling flux. Subsequently, we sum over all wavelength bands to obtain the broadband short-wave net flux  $F^{\text{net}}$ . After repeating the MATCH-AOP and DISORT radiative transfer computations without any LAC, we can compute the radiative impact  $\Delta F$  of LAC according to

$$\Delta F = F^{\text{net}}(\text{with LAC}) - F^{\text{net}}(\text{without LAC}). \quad (3)$$

## 3 Results

### 3.1 LAC optical properties

Figure 3 presents  $C_{\text{abs}}$  (first row),  $\omega$  (second row),  $g$  (third row), and  $C_{\text{bak}}$  (fourth row) as a function of  $R_V$  and  $\lambda$ . The computations have been performed with the aggregate model using the superposition T-matrix method (Mackowski and Mishchenko, 1996) (left column) and with the HSA using Lorenz-Mie theory (right column). Comparing the colour scales, one immediately notes that the results for  $C_{\text{abs}}$  computed with the aggregate model (panel a) are much higher than those computed with the HSA (b). The physical reason is that the electromagnetic field is unable to penetrate deeply into a massive LAC sphere consisting of highly absorbing material. As a consequence, much of the mass inside the homogeneous LAC spheres does not contribute to the mass absorption cross section. By contrast, the geometry of the fractal aggregates is such that most of the LAC mass can interact with the electromagnetic radiation.

Comparison of panels (c) and (d) shows that the HSA overestimates  $\omega$  over a large part of the size and wavelength ranges. At the same time, comparison of panels (e) and (f) shows that, at least at visible wavelengths, the HSA tends to underestimate  $g$ , so it overestimates the significance of side- and backscattering. We therefore expect that over a broad spectral range, the HSA will predict too little radiative

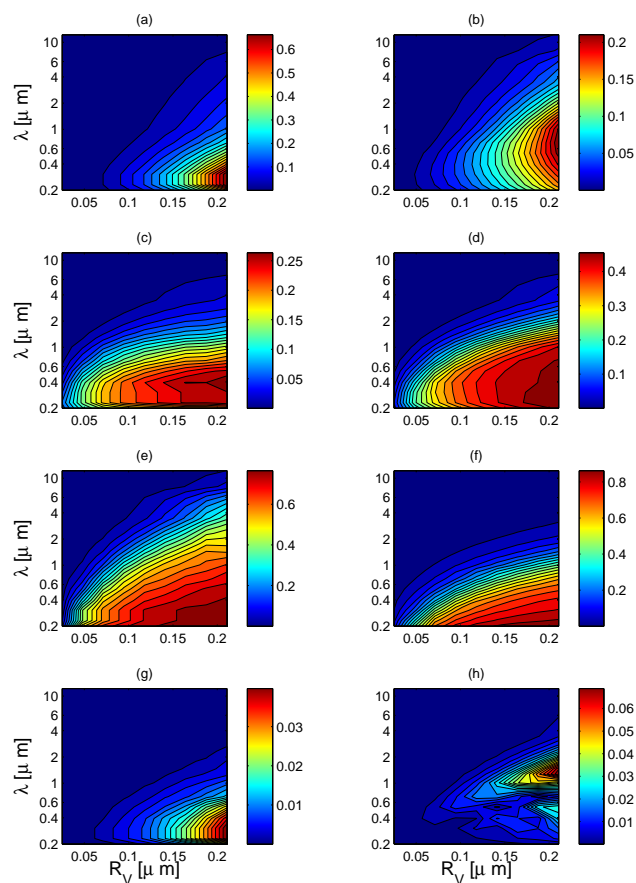


**Fig. 3.** AOPs of LAC computed with the aggregate model (left row) and with the HSA (right row) as a function of volume-equivalent radius  $R_V$  and wavelength  $\lambda$ . The panels show  $C_{\text{abs}}$  (first row),  $\omega$  (second row),  $g$  (third row), and  $C_{\text{bak}}$  (fourth row).

warming owing to the combined effect of an underestimation of absorption and an overestimation of the significance of total scattering in general and side- and backscattering in particular. A comparison of panel (g) and (h) reveals that the aggregate model and the HSA yield very different qualitative and quantitative predictions for  $C_{\text{bak}}$  and its dependency on size and wavelength. In particular, the aggregate model predicts the largest values of  $C_{\text{bak}}$  at UV and visible wavelengths, whereas the HSA yields the largest values of  $C_{\text{bak}}$  at NIR wavelengths.

The asymmetry parameter is the first Legendre moment of the phase function. This quantity may be less intuitively appealing than the phase function, which represents the normalised angular distribution of the scattered radiation. Thus the misrepresentation of the asymmetry parameter by the HSA may become clearer if we compare the phase functions computed with the two different models. The phase function depends on  $\lambda$ ,  $R_V$ , and on the scattering angle  $\Theta$ . To visualise this four-dimensional functional relation in a contour plot, we need to eliminate one of the independent variables.

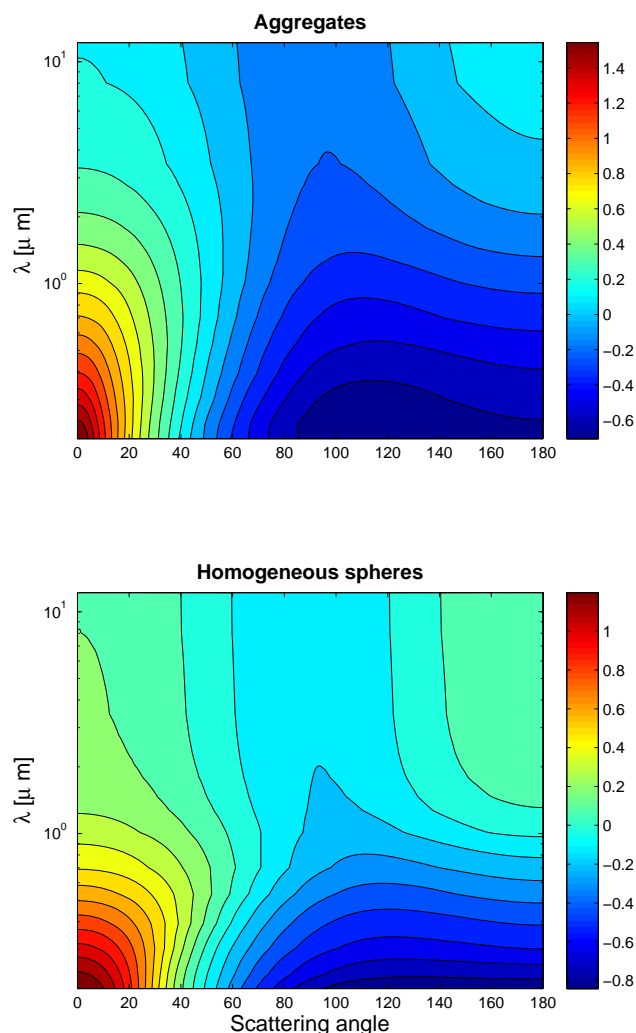


**Fig. 4.** Phase function  $p_\lambda(\Theta)$  as a function of scattering angle  $\Theta$  and wavelength  $\lambda$ . The phase functions are computed with the aggregate model (top) and the HSA (bottom), and size-averaged over a log-normal distribution.

We choose to eliminate the dependence on  $R_V$  by integrating over a fixed log-normal size distribution

$$n(R_V) = \frac{1}{R_V \sigma \sqrt{2\pi}} \exp\left[-\frac{\ln^2(R_V/R_V^0)}{2\sigma^2}\right], \quad (4)$$

where we assume  $R_V^0 = 52 \text{ nm}$  and  $\sigma = 0.42$ , which are obtained by fitting measurements of diesel soot emissions (Färnlund et al., 2001).

The spectral dependency of the size-averaged phase functions is shown in Fig. 4 for the aggregate model (top) and the HSA (bottom). One clearly sees that at visible and NIR wavelengths the aggregate model gives stronger and narrower forward-scattering peaks and less side- and backscattering, which explains why the aggregate model predicts larger asymmetry parameters at these wavelengths. At

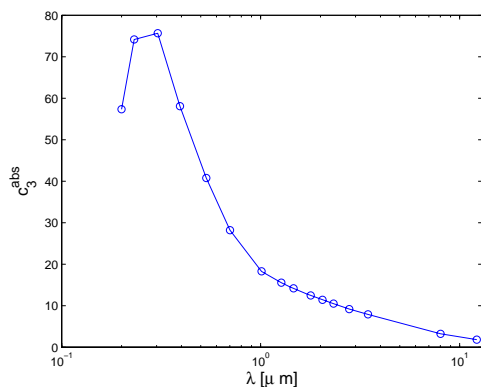


Fig. 5. Spectral dependency of the cubic fitting coefficient of  $C_{\text{abs}}$ .

wavelengths larger than  $6\mu\text{m}$  the phase function in either model approaches the Rayleigh limit, in which the phase function becomes more symmetric about the side scattering direction  $\Theta=90^\circ$ . The Rayleigh phase function has a minimum at  $\Theta=90^\circ$  and displays equally much forward as backward scattering, so  $g=0$ , which is what we see in Fig. 3 panels (e) and (f).

### 3.2 Implementation in MATCH

Next we need to consider how to efficiently couple the results from the electromagnetic scattering computations to dynamic 3-D aerosol fields computed with the MATCH model. It has been proposed (Kahnert, 2010a) to model the size-dependency of the AOPs of LAC by simple cubic fitting polynomials, i.e.

$$\text{AOP} = c_0 + c_1 R_V + c_2 R_V^2 + c_3 R_V^3. \quad (5)$$

With such an approach, averaging AOPs over the aerosol size distribution computed with a CTM reduces to computing the moments of the size distribution. For sectional or log-normal size distributions, the moments can be computed analytically.

For the aggregate model  $C_{\text{abs}}$  has been found to be proportional to the mass per particle (Kahnert (2010a,b), see also Liu and Mishchenko (2005)). Thus the size-dependency of  $C_{\text{abs}}$  can simply be fitted by

$$C_{\text{abs}} = c_3^{\text{abs}} R_V^3, \quad (6)$$

where the coefficient  $c_3^{\text{abs}}$  is defined by this equation. In this study we find that this relation holds over the entire spectral range. An example for the fitted size-dependency of  $C_{\text{abs}}$  is represented by the red line in Fig. 2 (upper left panel). Figure 5 shows that  $c_3^{\text{abs}}$  is a smooth function of wavelength. It would therefore be possible to find a suitable fitting function for  $c_3^{\text{abs}}$ , thus obtaining a two-dimensional parametrisation of  $C_{\text{abs}}(R_V, \lambda)$ .

For all AOPs other than  $C_{\text{abs}}$ , the empirical ansatz given in Eq. (5), which was found to work well at visible wavelengths,

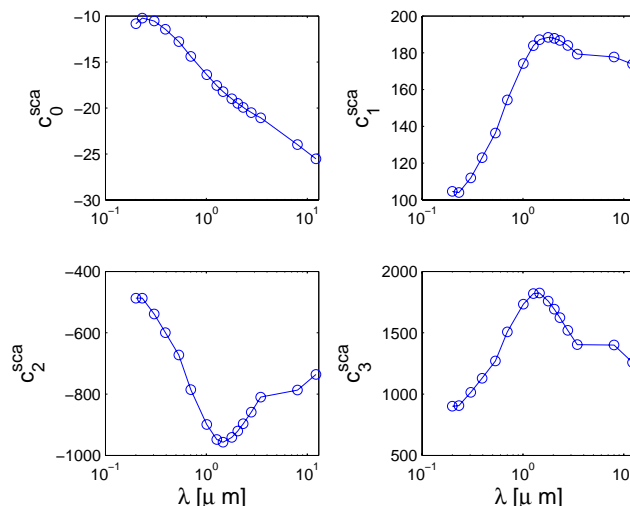


Fig. 6. Spectral dependency of the cubic fitting coefficients of  $C_{\text{sca}}$ .

turns out to be inaccurate at IR wavelengths. However, the cubic fitting ansatz works well for the natural logarithms of the AOPs, i.e.

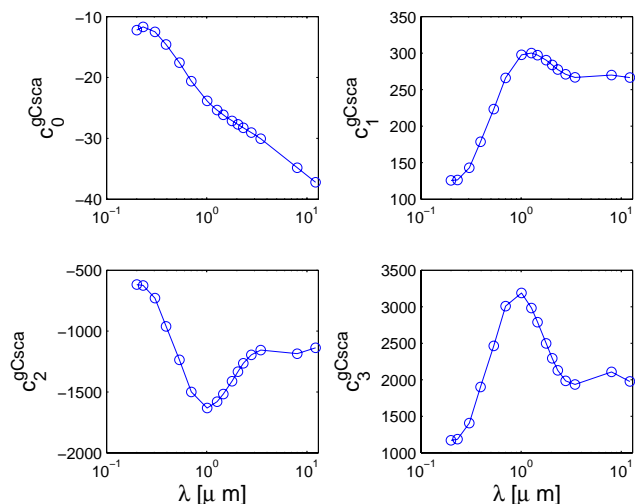
$$\ln \text{AOP} = c_0 + c_1 R_V + c_2 R_V^2 + c_3 R_V^3. \quad (7)$$

Figure 2 (red lines) gives examples for the fitting of  $\ln C_{\text{sca}}$  (upper right),  $\ln(g \times C_{\text{sca}})$  (lower left), and  $\ln C_{\text{bak}}$  (lower right).

Figures 6–8 show spectral dependencies of the fitting parameters for  $C_{\text{sca}}$ ,  $g \times C_{\text{sca}}$ , and  $C_{\text{bak}}$ , respectively. All of these coefficients are smooth functions of  $\lambda$ , so it would be possible to parametrise  $\ln \text{AOP}(R_V, \lambda)$  with respect to both arguments. However, given polynomial expressions for  $\ln \text{AOP}$  rather than for  $\text{AOP}$ , the computation of size-averaged AOPs now has to be done numerically. Therefore the fitting approach loses much of its appeal in broadband computations as compared to applications at visible wavelengths.

Instead it seems to be most straightforward to use the computed LAC AOPs directly in numerical size-integrations. This does not pose any technical problems in the CTM computations, as the size-averaged AOPs are computed off-line for the size bins used in the MATCH model. The pre-computed size-averaged AOPs are then read in by MATCH, multiplied by the aerosol number densities computed for each size bin in each grid cell, and averaged over all size bins. As output, MATCH delivers (apart from 3-D fields of aerosol number distribution and size-resolved aerosol chemical composition) 2-D fields of aerosol extinction optical depth  $\tau$  and 3-D fields of extinction coefficient  $d\tau/dz$  ( $z$  = altitude), backscattering coefficient,  $\omega$ ,  $g$ , and transmission length/visibility.

As an example, Fig. 9 presents MATCH results in the lowest model layer (i.e. closest to the surface) of the total aerosol mass mixing ratio  $\text{PM}_{10}$  (upper left, i.e. the mass of all aerosols smaller than  $10\mu\text{m}$  in diameter), the



**Fig. 7.** As Fig 5, but for  $g \times C_{\text{sca}}$ .

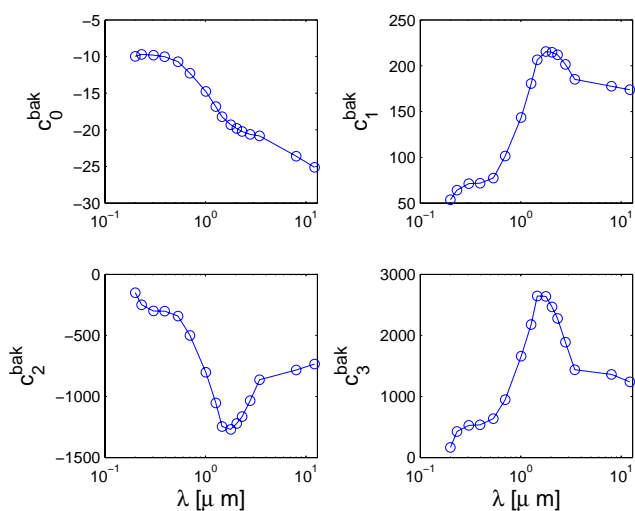


**Fig. 8.** As Fig 5, but for  $C_{\text{bak}}$ .

extinction coefficient (upper right),  $\omega$  (lower left), and  $g$  (lower right). The optical parameters are shown for a wavelength of 533.2 nm. The geographic distribution of the extinction coefficient correlates well with that of the PM<sub>10</sub> mass mixing ratios. High extinction coefficients are obtained over the ocean, where the aerosol mass is dominated by sea salt. Most of the sea salt mass is found in the coarse mode, which is characterised by high asymmetry parameters and, at visible wavelengths, single scattering albedos near unity (since sea salt is non-absorbing at visible wavelengths). Continental air pollution lowers the asymmetry parameter and, even more so, the single scattering albedo. Note the particularly low values of  $\omega$  around urban centres, such as Paris, London, Madrid, and even Stockholm. This is mainly caused by LAC emissions. Owing to the high absorption cross section, LAC emissions strongly lower the ensemble-averaged single

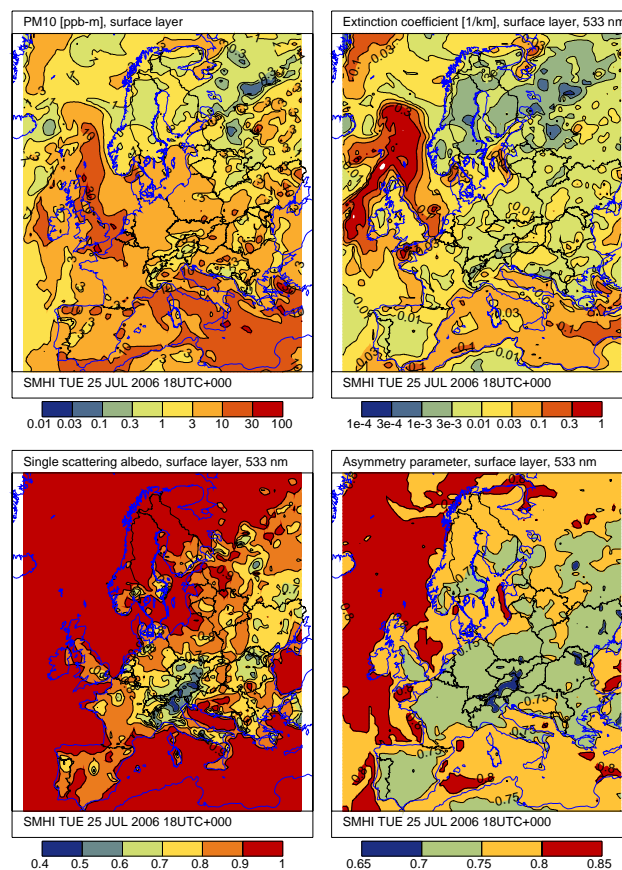


**Fig. 9.** PM<sub>10</sub> mass mixing ratio (upper left), extinction coefficient (upper right), single scattering albedo (lower left), and asymmetry parameter (lower right) on 25 July 2006, 18:00 UTC. The optical parameters are shown for  $\lambda=533.2$  nm. All results are shown for the model layer closest to the surface.

scattering albedo. By contrast, the asymmetry parameter  $g$  displays much less geographic fine structure as compared to  $\omega$ . The asymmetry parameter of LAC does not differ dramatically from that of other anthropogenic aerosols. The lower values of  $g$  over the continent can be explained by the fact that continental aerosols are dominated by particles in the accumulation mode, which scatter light more isotropically than coarse mode particles. Coarse sea salt aerosols are usually quickly deposited over land.

### 3.3 Radiative transfer computations

We want to obtain a rough estimate of the error caused by the HSA in broadband radiative forcing calculations. To this end we pick from the 3-D fields of size-averaged spectral AOPs a 1-D vertical profile at a latitude of 48.2° N and a longitude of 2.3° E computed for 25 July 2006. Radiative transfer computations are performed for a solar zenith angle of 35°. This test case has been previously considered in the *spectral* radiative impact estimates discussed by Kahnert (2010a). For this

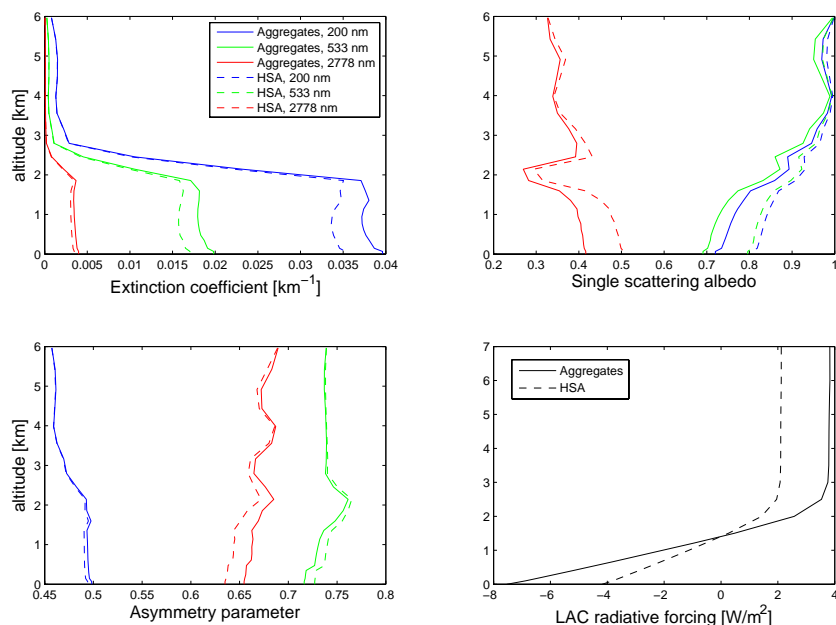


**Fig. 10.** Vertical profiles of extinction coefficient (upper left),  $\omega$  (upper right),  $g$  (lower left), and shortwave radiative impact (lower right) computed for 25 June 2006 at a latitude of  $48.2^\circ$  N and a longitude of  $2.3^\circ$  E. The curves display computational results based on the aggregate model (solid lines) and on the HSA (dashed lines). Broadband results are represented by black lines, spectral results by blue lines (200 nm), green lines (533 nm), and red lines (2778 nm).

test case, Fig. 10 shows  $d\tau/dz$  (upper left),  $\omega$  (upper right), and  $g$  (lower left) as a function of altitude  $z$ . Results for the aggregate model (solid lines) and the HSA (dashed lines) are presented for three wavelengths, namely 200 nm (blue lines), 533 nm (green lines), and 2778 nm (red lines).

The lower right panel in Fig. 10 shows the LAC broadband radiative impact  $\Delta F$  as a function of altitude computed with the aggregate model using the superposition T-matrix method (solid line) and with the HSA using Lorenz-Mie theory (dashed line). At the surface the radiative impact computed with the aggregate model is nearly  $-8 \text{ W/m}^2$ , whereas the HSA predicts only a radiative impact of  $-4 \text{ W/m}^2$ . Above the aerosol layer, The aggregate model gives  $\Delta F=4 \text{ W/m}^2$ , whereas the HSA predicts only  $\Delta F=2 \text{ W/m}^2$ . In either case, the absolute value of the radiative impact computed with the aggregate model is approximately a factor of 2 larger than that computed with the HSA. This is a remarkable result that highlights the importance of accounting for particle morphology in assessing the direct radiative forcing effect of externally mixed LAC aggregates.

#### 4 Conclusions

Size-dependent optical properties of LAC aggregates have been computed for the wavelength range from 200 nm up to  $12.2 \mu\text{m}$  by use of the numerically exact superposition T-matrix solution to the electromagnetic scattering problem.

The optical properties have been integrated into the chemical transport model MATCH. This allows us to compute 3-D fields of size-averaged aerosol optical properties. Such computational results have been employed as input to a radiative transfer model, from which we obtain the radiative impact of LAC. The aggregate model predicts a shortwave radiative impact that is twice as high as that computed with the homogeneous sphere model. It is therefore possible that previous studies have substantially underestimated the net-warming effect of LAC.

Although a precise quantification of the HSA-error in LAC forcing computations will require application of the aggregate model in a global climate model and an extended time-integration, the results obtained here provide a clear indication for the inadequacy of the homogeneous sphere approximation in LAC climate forcing computations. Realistic estimates of the LAC forcing effect will further need to take internal mixing of aged LAC aerosols with soluble compounds, such as sulphate, into account. Internal mixing is known to further enhance the radiative forcing effect of LAC (Bond et al., 2006).

As demonstrated in this study, it is fairly straightforward to couple the AOPs computed with the aggregate model to a CTM. Thus the AOPs can be readily implemented in an Earth-system model, in which an atmosphere-ocean GCM is coupled to a CTM. One such Earth-system model is the coupled atmosphere-ocean-chemistry-vegetation model EC-EARTH, which is based on IFS. The LAC optics

computations in our study have been tailored to the 14-band radiation scheme employed in the newer versions of IFS.

On-line computations of ensemble-averaged AOPs in a CTM or an Earth-system model based on an off-line computed look-up table requires only little computation time in comparison to that needed for computing chemical and meteorological processes. However, the computational effort to create an AOP look-up table in the first place can be quite substantial, since electromagnetic scattering computations for such complex particles as fractal aggregates tend to be very time consuming. The computations presented in the left column of Fig. 3 took several weeks of wallclock-time. The main reason why it was still possible to perform computations based on rigorous theory over such an extensive range of particle sizes and wavelengths is the fact that the optical properties of LAC aggregates are rather smooth functions of  $R_V$  and  $\lambda$ . The optical properties of other aerosol species, such as mineral aerosols, often display oscillations with size and wavelength, which are caused by internal optical resonances inside the particles and by surface waves. To resolve these oscillations, one usually has to perform AOP computations for a large number of discrete sizes and wavelengths. By contrast, LAC aggregates are composed of highly absorbing material, which quenches the optical resonances. For this reason it is sufficient to limit AOP computations to a manageable number of sizes and wavelengths. Results at other sizes or wavelengths can be obtained by interpolation.

*Acknowledgements.* The author thanks D. Mackowski for providing his program for aggregated-particle generation. D. Mackowski and M. Mishchenko are acknowledged for making their superposition T-matrix program publicly available. Y. Okada and A. Kokhanovsky are acknowledged for making their numerical orientational averaging routines publicly available. This work was supported by the Swedish Research Council under contract number 80438701.

Edited by: Y. Balkanski

## References

- Andersson, C., Langner, J., and Bergström, R.: Interannual variation and trends in air pollution over Europe due to climate variability during 1958–2001 simulated with a regional CTM coupled to the ERA40 reanalysis, *Tellus*, 59B, 77–98, 2007.
- Bond, T. C. and Bergstrom, R. W.: Light absorption by carbonaceous particles: An investigative review, *Aerosol Sci. Technol.*, 40, 27–67, 2006.
- Bond, T. C., Habib, G., and Bergstrom, R. W.: Limitations in the enhancement of visible light absorption due to mixing state, *J. Geophys. Res.*, 111, D20211, doi:10.1029/2006JD007315, 2006.
- Bruggemann, D. A. G.: Berechnung verschiedener physikalischer Konstanten von heterogenen Substanzen. 1. Dielektrizitätskonstanten und Leitfähigkeiten der Mischkörper aus isotropen Substanzen, *Ann. Phys.*, 24, 636–664, 1935.
- Chang, H. and Charalampopoulos, T. T.: Determination of the wavelength dependence of refractive indices of flame soot, *Proc. R. Soc. Lond. A*, 430, 577–591, 1990.
- Färnlund, J., Holman, C., and Kågeson, P.: Emissions of ultra-fine particles from different types of light duty vehicles, *Tech. Rep. 2001:10*, Swedish National Road Administration, Borlänge, 2001.
- Forster, P., Ramaswamy, V., Artaxo, P., Berntsen, T., Betts, R., Fahey, D. W., Haywood, J., Lean, J., Lowe, D. C., Myhre, G., Nganga, J., Prinn, R., Raga, G., Schulz, M., and Van Dorland, R.: Changes in atmospheric constituents and in radiative forcing., in: *Climate Change 2007: The Physical Science Basis.*, edited by Solomon, S., Qin, D., Manning, M., Chen, Z., Marquis, M., Averyt, K. B., Tignor, M., and Miller, H. L., Contribution of Working Group I to the Fourth Assessment Report of the Intergovernmental Panel on Climate Change, Cambridge University Press, Cambridge, 153–234, 2007.
- Fuller, K. A.: Scattering and absorption cross sections of compounded spheres III. Spheres containing arbitrarily located spherical inhomogeneities, *J. Opt. Soc. Am. A*, 12, 893–904, 1995.
- Fuller, K. A., Malm, W. C., and Kreidenweis, S. M.: Effects of mixing on extinction by carbonaceous particles, *J. Geophys. Res.*, 104, 15941–15954, 1999.
- Jacobson, M. Z.: A physically-based treatment of elemental carbon optics: Implications for global direct forcing of aerosols, *Geophys. Res. Lett.*, 27, 217–220, 2000.
- Jacobson, M. Z.: Strong radiative heating due to the mixing state of black carbon in atmospheric aerosols, *Nature*, 409, 695–697, 2001.
- Kahnert, F. M.: Reproducing the optical properties of fine desert dust aerosols using ensembles of simple model particles, *J. Quant. Spectrosc. Radiat. T.*, 85, 231–249, 2004.
- Kahnert, M.: Modelling the optical and radiative properties of freshly emitted light absorbing carbon within an atmospheric chemical transport model, *Atmos. Chem. Phys.*, 10, 1403–1416, doi:10.5194/acp-10-1403-2010, 2010a.
- Kahnert, M.: On the discrepancy between modelled and measured mass absorption cross sections of light absorbing carbon aerosols, *Aerosol Sci. Technol.*, 44, 453–460, 2010b.
- Kahnert, M. and Kylling, A.: Radiance and flux simulations for mineral dust aerosols: Assessing the error due to using spherical or spheroidal model particles, *J. Geophys. Res.*, 109, D09203, doi:10.1029/2003JD004318, 2004.
- Kahnert, M. and Nousiainen, T.: Uncertainties in measured and modelled asymmetry parameters of mineral dust aerosols, *J. Quant. Spectrosc. Radiat. T.*, 100, 173–178, 2006.
- Kahnert, M., Nousiainen, T., and Veihelmann, B.: Spherical and spheroidal model particles as an error source in aerosol climate forcing and radiance computations: A case study for feldspar aerosols, *J. Geophys. Res.*, 110, D18S13, doi:10.1029/2004JD005558, 2005.
- Kahnert, M., Nousiainen, T., and Räisänen, P.: Mie simulations as an error source in mineral aerosol radiative forcing calculations, *Q. J. Roy. Meteor. Soc.*, 133, 299–307, 2007.
- Kocifaj, M. and Videen, G.: Optical behavior of composite carbonaceous aerosols: DDA and EMT approaches, *J. Quant. Spectrosc. Radiat. T.*, 109, 1404–1416, 2008.
- Liu, L. and Mishchenko, M. I.: Effects of aggregation on scattering

- and radiative properties of soot aerosols, *J. Geophys. Res.*, 110, D11211, doi:10.1029/2004JD005649, 2005.
- Liu, L., Mishchenko, M. I., and Arnott, W. P.: A study of radiative properties of fractal soot aggregates using the superposition  $T$ -matrix method, *J. Quant. Spectrosc. Radiat. T.*, 109, 2656–2663, 2008.
- Mackowski, D. W.: Calculation of total cross sections of multiple-sphere clusters, *J. Opt. Soc. Am. A*, 11, 2851–2861, 1994.
- Mackowski, D. W. and Mishchenko, M. I.: Calculation of the  $T$  matrix and the scattering matrix for ensembles of spheres, *J. Opt. Soc. Am. A*, 13, 2266–2278, 1996.
- Maxwell-Garnett, J. C.: Colours in metal glasses and in metallic films, *Philos. Trans. R. Soc. A*, 203, 385–420, 1904.
- Mishchenko, M. I., Liu, L., Travis, L. D., and Lacis, A. A.: Scattering and radiative properties of semi-external versus external mixtures of different aerosol types, *J. Quant. Spectrosc. Radiat. T.*, 88, 139–147, 2004.
- Okada, Y. and Kokhanovsky, A. A.: Light scattering and absorption by densely packed groups of spherical particles, *J. Quant. Spectrosc. Radiat. T.*, 110, 902–917, 2009.
- Okada, Y., Mann, I., Mukai, T., and Köhler, M.: Extended calculation of polarization and intensity of fractal aggregates based on rigorous method for light scattering simulations with numerical orientation averaging, *J. Quant. Spectrosc. Radiat. T.*, 109, 2613–2627, 2008.
- Otto, S., Bierwirth, E., Weinzierl, B., Kandler, K., Esselborn, M., Tesche, M., Schladitz, A., Wendisch, M., and Trautmann, T.: Solar radiative effects of a Saharan dust plume observed during SAMUM assuming spheroidal model particles, *Tellus*, 61B, 270–296, 2009.
- Pilinis, C. and Li, X.: Particle shape and internal inhomogeneity effects in the optical properties of tropospheric aerosols of relevance to climate forcing, *J. Geophys. Res.*, 103, 3789–3800, 1998.
- Ramanathan, V. and Carmichael, G.: Global and regional climate changes due to black carbon, *Nature Geosci.*, 1, 221–227, 2008.
- Schulz, F. M. and Stamnes, K.: Angular distribution of the Stokes vector in a plane parallel, vertically inhomogeneous medium in the vector discrete ordinate radiative transfer (VDISORT) model, *J. Quant. Spectrosc. Radiat. T.*, 65, 609–620, 2000.
- Schulz, F. M., Stamnes, K., and Stamnes, J. J.: Modeling the radiative transfer properties of media containing particles of moderately and highly elongated shape, *Geophys. Res. Lett.*, 25, 4481–4484, 1998.
- Schulz, F. M., Stamnes, K., and Stamnes, J. J.: Shape-dependence of the optical properties in size-shape distributions of randomly oriented prolate spheroids, including highly elongated shapes, *J. Geophys. Res.*, 104, 9413–9421, 1999a.
- Schulz, F. M., Stamnes, K., and Weng, F.: VDISORT: An improved and generalized discrete ordinate radiative transfer model for polarized (vector) radiative transfer computations, *J. Quant. Spectrosc. Radiat. T.*, 61, 105–122, 1999b.
- Sorensen, C. M.: Light scattering by fractal aggregates: A review, *Aerosol Sci. Technol.*, 35, 648–687, 2001.
- Sorensen, C. M. and Roberts, G. M.: The prefactor of fractal aggregates, *J. Colloid. Interface Sci.*, 186, 447–452, 1997.
- Stamnes, K., Tsay, S.-C., Wiscombe, W., and Jayaweera, K.: Numerically stable algorithm for discrete-ordinate-method radiative transfer in multiple scattering and emitting layered media, *Appl. Opt.*, 27, 2502–2509, 1988.
- Veihelmann, B., Nousiainen, T., Kahnert, M., and van der Zande, W. J.: Light scattering by small feldspar particles simulated using the Gaussian random sphere geometry, *J. Quant. Spectrosc. Radiat. T.*, 100, 393–405, 2006.
- Videen, G. and Chýlek, P.: Scattering by a composite sphere with an absorbing inclusion and effective medium approximations, *Opt. Commun.*, 158, 1–6, 1998.
- Weng, F.: A multi-layer discrete-ordinate method for vector radiative transfer in a vertically-inhomogeneous, emitting and scattering atmosphere—I. theory, *J. Quant. Spectrosc. Radiat. T.*, 47, 19–33, 1992.
- Worringen, A., Ebert, M., Trautmann, T., Weinbruch, S., and Helas, G.: Optical properties of internally mixed ammonium sulfate and soot particles—a study of individual aerosol particles and ambient aerosol populations, *Appl. Opt.*, 47, 3835–3845, 2008.
- Xu, Y. and Gustafson, B. Å. S.: A generalized multiparticle Mie-solution: further experimental verification, *J. Quant. Spectrosc. Radiat. Transfer*, 70, 395–419, 2001.
- Zhao, Y. and Ma, L.: Assessment of two fractal scattering models for the prediction of the optical characteristics of soot aggregates, *J. Quant. Spectrosc. Radiat. T.*, 110, 315–322, 2009.